Available at
www.ComputerScienceWeb.com
POWERED BY SCIENCE DIRECT

Signal Processing 83 (2003) 2469–2480

SIGNAL PROCESSING

www.elsevier.com/locate/sigpro

Acoustic wave propagation in a 1-D lattice: analysis of nonlinear effects by the fractional Fourier transform method

Gilles Gonon[a,*], Olivier Richoux[b], Claude Depollier[b]

[a] *Laboratoire d'Informatique, Université du Maine, Le Mans, Cedex 9 72085, France*
[b] *Laboratoire d'Acoustique, UMR CNRS 6613, Université du Maine, Le Mans, Cedex 9 72085, France*

Received 9 January 2003

Abstract

This article deals with a method based on the fractional Fourier transform (FRFT) to estimate the parameters of linear chirps. Appropriate filtering in fractional domains based on this method allows to extract linear chirps out of a multicomponent and noisy signal. This method is used to analyse the propagation of acoustic wave in a dispersive medium (lattice made up of Helmholtz resonators). The nonlinear effects due to the Helmholtz resonators are highlighted. The frequency dependance of the nonlinear processes is shown thanks to the extraction method proposed.

Keywords: Time–frequency; Fractional Fourier transform; Chirp; Estimation; Filtering

1. Introduction

Time–frequency analysis provides a major contribution to the analysis of nonstationary signals. Among time–frequency signal representations, the Wigner–Ville distribution, denoted WVD, is suitable to the analysis of linear chirp signals. However, due to its nonlinear character, the WVD induces interference terms that disturb the readability of the distribution, in the case of multicomponent signals. Thus, there is a need to use different methods that locally emphasize signal concentration and improve parameter estimation. We present here a method based on the fractional Fourier transform (FRFT) to extract linear chirps out of a multicomponent and noisy signal and estimate their parameters. The FRFT is related to other time–frequency representations and allows perfect reconstruction of a signal. More specifically, its equivalence to the Radon Transform shows that the FRFT projects the time–frequency distribution of the signal onto rotating slices.

This extraction method is applied to an experimental acoustic signal. The analysed signal results from the propagation of an acoustic wave through a lattice made up of Helmholtz resonators. For high levels of the source, the response of the lattice is not linear and higher harmonics are generated by interactions of acoustic wave with the resonators. A linear FM (chirp) signal is used to emphasize the time–frequency behaviour of the lattice response. The harmonic components are separated by filtering in appropriate fractional domains

* Corresponding author.
E-mail addresses: gilles.gonon@univ-lemans.fr (G. Gonon), olivier.richoux@univ-lemans.fr (O. Richoux), claude.depollier@univ-lemans.fr (C. Depollier).

0165-1684/$ - see front matter © 2003 Elsevier B.V. All rights reserved.
doi:10.1016/j.sigpro.2003.05.001

and then each wave is recovered via inverse transform.

Section 2 recalls the definition and properties of the FRFT and presents the extraction method of linear chirps. Section 3 introduces the theory for the acoustic propagation in the lattice and provides a nonlinear model of the response of the Helmholtz resonators. The experimental setup is presented and the experimental results are discussed in Section 4.

2. Linear chirp analysis with the FRFT

2.1. The fractional Fourier transform (FRFT)

The FRFT was introduced by Namias [6] in the framework of quantum mechanics where it provides an efficient tool to solve some classes of differential equations. Since this work, discrete algorithms were implemented [7] and several applications of the FRFT have been suggested and developed mostly related to optic applications.

2.1.1. Definition and properties

The αth order FRFT of a function denoted by $\{\mathscr{F}^{\alpha}x\}(t_\alpha)$ is defined for $\alpha\in[0,4]$ by

$$\{\mathscr{F}^{\alpha}x\}(t_\alpha)=x_\alpha(t_\alpha)=\int_{-\infty}^{\infty}\mathscr{K}_\alpha(t_\alpha,t)x(t)\,\mathrm{d}t, \tag{1}$$

where the kernel set of functions $\mathscr{K}_\alpha(t_\alpha,t)$ is

$$\mathscr{K}_\alpha(t_\alpha,t)=\begin{cases}A_\phi \mathrm{e}^{\mathrm{j}\pi((t_\alpha^2+t^2)\cot\phi-(2t_\alpha t/\sin\phi)} & \text{if } \phi\neq n\pi,\ n\in Z,\\ \delta(t-t_\alpha) & \text{if } \phi=2\pi n,\\ \delta(t+t_\alpha) & \text{if } \phi+\pi=2\pi n.\end{cases} \tag{2}$$

with $\phi=\alpha(\pi/2)$, $(j)^2=-1$ and

$$A_\phi=\frac{\exp[-\mathrm{j}\pi\,\mathrm{sgn}(\sin\phi/4)+\mathrm{j}\,\frac{\phi}{2}]}{\sqrt{|\sin\phi|}}. \tag{3}$$

The kernel functions taken as functions of t_α with parameter t belong to an orthonormal set and form a one parameter group:

$$\int_{-\infty}^{\infty}\mathscr{K}_\alpha(t_\alpha,t)\mathscr{K}_\alpha^*(t_\alpha,t')\,\mathrm{d}t_\alpha=\delta(t-t'), \tag{4}$$

$$\int_{-\infty}^{\infty}\mathscr{K}_\alpha(t_\alpha,t')\mathscr{K}_\beta(t',t)\,\mathrm{d}t'=\mathscr{K}_{\alpha+\beta}(t_\alpha,t). \tag{5}$$

Letting the superscript $*$ represent the complex conjugation operation, the kernel functions verify the following properties:

$$\mathscr{K}_\alpha(t_\alpha,t)=\mathscr{K}_\alpha(t,t_\alpha),$$

$$\mathscr{K}_{-\alpha}(t_\alpha,t)=\mathscr{K}_\alpha^*(t_\alpha,t),$$

$$\mathscr{K}_\alpha(-t_\alpha,t)=\mathscr{K}_\alpha(t_\alpha,-t).$$

The inverse transform can be derived from these properties as

$$x(t)=\int\mathscr{K}_{-\alpha}(t_\alpha,t)[\{\mathscr{F}^{\alpha}x\}(t_\alpha)]\,\mathrm{d}t_\alpha. \tag{6}$$

The properties of the FRFT are directly deduced from the kernel functions. The most important properties are the following:

- it is linear; the first order transform ($\alpha=1$) corresponds to the common Fourier transform,
- continuity in α, which means that a signal can evolve continuously from time to frequency.
- commutativity: $\mathscr{F}^{\alpha_1}[\mathscr{F}^{\alpha_2}[S(t)]]=\mathscr{F}^{\alpha_2}[\mathscr{F}^{\alpha_1}[S(t)]]$;
- composition of transform: $\mathscr{F}^{\alpha_1}[\mathscr{F}^{\alpha_2}[S(t)]]=\mathscr{F}^{\alpha_1+\alpha_2}[S(t)]$;
- it is a unitary transform, implying Parseval's identity (perfect reconstruction).

2.1.2. Relationship with other time–frequency transforms

The group property of the $\mathscr{K}_\alpha(t_\alpha,t)$ functions and the particular cases $\alpha=0$ and $\alpha=1$ result in the interpretation of the FRFT as the signal distribution along a fractional domain t_α between time and frequency. In fact the FRFT is related to the Wigner distribution [1]. As it is well known, the Wigner distribution $W_x(t,f)$ of the function $x(t)$ defined by

$$W_x(t,f)=\int_{-\infty}^{\infty}\mathrm{e}^{-\mathrm{j}2\pi f\tau}x\left(t+\frac{\tau}{2}\right)x^*\left(t-\frac{\tau}{2}\right)\,\mathrm{d}\tau \tag{7}$$

is the time–frequency energy distribution of the signal and its projection onto the t (resp.f) axis gives the magnitude squared of the time (resp. frequency) domain representation:

$$\int_{-\infty}^{\infty} W_x(t,f)\,\mathrm{d}f = |x(t)|^2,$$

$$\int_{-\infty}^{\infty} W_x(t,f)\,\mathrm{d}t = |x_1(f)|^2, \tag{8}$$

where $x_1(f)$ is the Fourier transform of $x(t)$. Such a property can be extended to the fractional domains through the relationship between the FRFT and the Radon transform. The Radon transform operator, denoted $\mathscr{R}_\phi$, takes the integral projection of the function $W_x(t,f)$ onto an axis making angle ϕ with the t axis. It is defined by

$$\mathscr{R}_\phi[W_x(t,f)] = \int_{-\infty}^{+\infty} W_x(r\cos\phi - u\sin\phi, r\sin\phi + u\cos\phi)\,\mathrm{d}u, \tag{9}$$

where $r = t\cos\phi + f\sin\phi$ and $u = -t\sin\phi + f\cos\phi$.

The generalization of property (8) for any fractional domain, shown in [3], leads to the following relation:

$$\mathscr{R}_\phi[W_x(t,f)] = |x_\alpha(t_\alpha)|^2, \tag{10}$$

This relationship to the radon transform emphasizes two results about the FRFT: it acts as a rotational operator according to α in the time–frequency plane and for a given α it expands the signal on a linear chirp basis, as the traditional Fourier transform expands a signal on a sinusoidal basis. These results are developed in the next section.

2.2. Linear chirp FRFT

A linear chirp, denoted by $\mathscr{C}$, follows the temporal equation $\mathscr{C}(t) = \mathrm{e}^{\mathrm{j}(\omega_0 t + \tan\phi t^2)}$. Its ideal time–frequency distribution is a line with the slope $\tan\phi$, as shown in Fig. 1. Such a signal is fully defined by two parameters being the frequency offset at the origin ω_0 and ϕ.

2.2.1. Theoretical case

According to Fig. 1, the geometrical interpretation of the FRFT as a projection on a rotating axis in the time–frequency plane leads to the result that the chirp projection will provide maximal concentration for angle $\phi+\pi/2$ corresponding to an order $\alpha+1$. Analytical

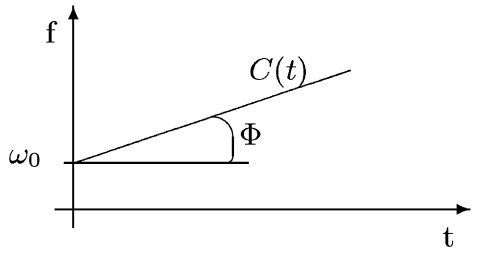

Fig. 1. Linear chirp theoretical time–frequency distribution.

derivation confirms that result. The FRFT of $\mathscr{C}$ at order $\alpha+1$ leads to the following transform, assuming definition (1):

$$\mathscr{C}_{\alpha+1}(t_{\alpha+1}) = A_{\phi+(\pi/2)}\mathrm{e}^{\mathrm{j}\pi\cot(\phi+(\pi/2))t_{\alpha+1}^2}\int_{-\infty}^{+\infty}\mathrm{e}^{\mathrm{j}\pi(\omega_0 t+\tan\phi t^2)} \times \mathrm{e}^{\mathrm{j}\pi(t^2\cot(\phi+(\pi/2))-(2t_{\alpha+1}t)/(\sin(\phi+(\pi/2))))}\,\mathrm{d}t. \tag{11}$$

As $\sin(\phi+(\pi/2)) = \cos\phi$ and $\cot(\phi+(\pi/2)) = -\tan\phi$, quadratic terms of the integrand cancel each other, leading to

$$\mathscr{C}_{\alpha+1}(t_{\alpha+1}) = A_{\phi+(\pi/2)}\mathrm{e}^{\mathrm{j}\pi\tan\phi t_{\alpha+1}^2} \times \int_{-\infty}^{+\infty}\mathrm{e}^{2\mathrm{j}\pi((\omega_0/2)-(t_{\alpha+1}/\cos\phi))t}\,\mathrm{d}t. \tag{12}$$

Then applying the variable change $t' = t/\cos\phi \rightarrow \cos\phi\,\mathrm{d}t' = t$ leads to the following Fourier transform:

$$\mathscr{C}_{\alpha+1}(t_{\alpha+1}) = A_{\phi+(\pi/2)}\cos\phi\,\mathrm{e}^{-\mathrm{j}\pi\tan\phi t_{\alpha+1}^2} \times \underbrace{\int_{-\infty}^{+\infty}\mathrm{e}^{-2\mathrm{j}\pi(\omega_0\cos\phi t'/2)}\mathrm{e}^{-2\mathrm{j}\pi t_{\alpha+1}t'}\,\mathrm{d}t'}. \tag{13}$$

The underbraced integral part is the Fourier transform of function $\mathrm{e}^{-2\mathrm{j}\pi(\omega_0\cos\phi t'/2)}$ and is equal to $\delta(t_{\alpha+1} - (\omega_0\cos\phi/2))$, so that Eq. (13) leads to the expected result:

$$\mathscr{C}_{\alpha+1}(t_{\alpha+1}) = A_{\phi+(\pi/2)}\cos\phi\,\mathrm{e}^{-(\mathrm{j}\pi\tan\phi t_{\alpha+1}^2)} \times \delta\left(t_{\alpha+1} - \frac{\omega_0\cos\phi}{2}\right). \tag{14}$$

Eq. (14) shows that the $\phi + (\pi/2)$ order FRFT of a chirp of slope ϕ is a Dirac function whose position depends on the frequency offset parameter of the chirp and whose magnitude depends on the order of the transform.

This result is due to the orthogonality of the kernel functions but also the orthogonality of domains t_α and $t_{\alpha+1}$. From Eq. (14) the linear chirp parameters can easily be estimated. The angle of the transform providing maximal concentration is perpendicular to ϕ and the Dirac position in the $t_{\alpha+1}$ domain leads to ω_0 through the relation $t_{\alpha+1} = (\omega_0 \cos\phi/2)$.

2.2.2. Windowed case

As any application deals with finite length signal, we present here the case of a windowed linear chirp. Let $W(t)$ denote a temporal window and $\mathscr{C}_W(t) = \mathscr{C}(t).W(t)$ denote the windowed signal. The FRFT of $\mathscr{C}_W$ at order $\alpha + 1$ follows the same derivation as in the latter section. The result is similar to the effect of a window on the Fourier transform of a signal, i.e. the Dirac function in Eq. (14) is convolved with the FT of the window.

As an example, we give the result of the FRFT of $\mathscr{C}_W$ in the case of the rectangle window with time support $[t_1, t_2]$ centred in k and denoted $1_{[t_1,t_2]}(t)$. The derivation can easily be adapted to other window types, starting from Eq. (13). In this case, the integral related to the rectangle window is

$$\int_{-\infty}^{+\infty} \mathrm{e}^{-2\mathrm{j}\pi(\omega_0 \cos\phi t'/2)}\, 1_{[t_1',t_2']}(t')\, \mathrm{e}^{-2\mathrm{j}\pi t_{\alpha+1} t'}\, \mathrm{d}t'$$
$$= \left[\delta\left(t_{\alpha+1} - \frac{\omega_0 \cos\phi}{2}\right) * \left(\frac{\sin 2\pi T' t_{\alpha+1}}{2\pi t_{\alpha+1}\, \mathrm{e}^{-\mathrm{j}2\pi k' t_{\alpha+1}}}\right)\right], \quad (15)$$

where $T = t_2 - t_1$, $t_1' = t_1/\cos\phi$, $t_2' = t_2/\cos\phi$, $T' = T/\cos\phi$, $k' = k/\cos\phi$.

Finally the FRFT of order $\alpha + 1$ of a linear chirp windowed by a rectangle window is

$$\mathscr{C}_{\alpha+1}(t_{\alpha+1}) = A_{\phi+(\pi/2)} \cos\phi\, \frac{\sin 2\pi T'(t_{\alpha+1} - (\omega_0 \cos\phi/2))}{2\pi(t_{\alpha+1} - (\omega_0 \cos\phi/2))} \times \mathrm{e}^{-\mathrm{j}\pi(t_{\alpha+1}^2 \tan\phi + (t_{\alpha+1} - (\omega_0 \cos\phi)/2)2k')}. \quad (16)$$

Eq. (16) provides the basic result for linear chirp analysis, estimation and localization. The analysis can be performed in three steps:

- *Chirp detection*: when sweeping the fractional domains within range $\alpha \in [0, 2]$ a chirp is detected each time a local maxima appears (threshold method), see Fig. 2.
- *Chirp estimation*: given an order α where a local maximum is found, the slope of the detected chirp is $\alpha - 1$. The offset is deduced from the ordinates $t_{\alpha+1}^{\max}$ of the maximum with the relation: $\omega_0 = 2t_{\alpha+1}^{\max}/\cos\phi$, see Fig. 3.
- *Chirp localization*: the length of the chirp can be estimated through the size of the main lobe, but this requires knowing the shape of the window applied to the signal. In that case, it is also possible to extract the central position of the window from the maximum of the FRFT phase. For the rectangle window, the main lobe size is $2\cos(\phi)/T$ and the expected phase is parabolic with maximum localized at $t_{\alpha+1} = k/\sin(\phi)$. Fig. 3 illustrates the estimation of the window parameters.

2.3. Filtering in fractional domains: chirp extraction

Thanks to the perfect reconstruction and linearity properties, the FRFT offers new perspective for filtering signal and noise. It becomes possible to filter different components in a signal that overlap both in the time and frequency domains but have disjoint support projections on a radial axis of the time–frequency plane.

Table 1 shows the results in terms of normalized mean square errors (MSE) for three kind of chirp filtering for various SNR. As these examples use simulated signals, the targeted signal T is known by definition and the normalized MSE for a N-tap signal S resulting from filtering is computed according to:

$$\mathrm{MSE} = \frac{\sum_{k=1}^{N} (T[k] - S[k])^2}{\sum_{k=1}^{N} (T[k])^2}. \quad (17)$$

For each case, filtering in an appropriate fractional domain is performed by keeping the coefficients relevant to a specific chirp and then returning in the temporal domain by inverse FRFT.

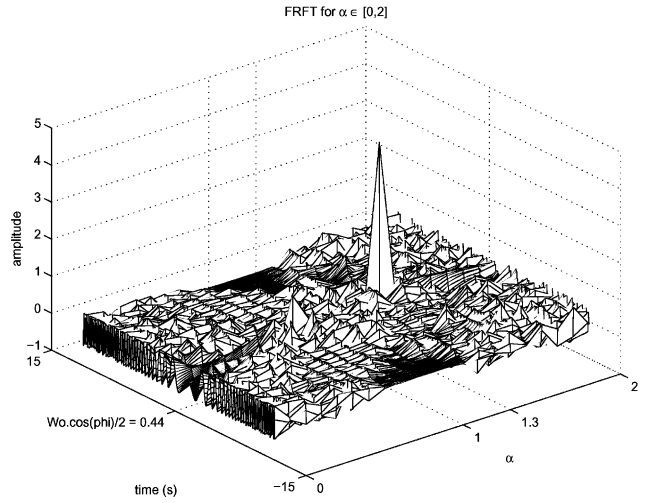

Fig. 2. FRFT of a linear chirp with parameters: slope $\tan(\alpha_0\pi/2)$ with $\alpha_0 = 0.3$ and offset $\omega_0 = 1$. α ranges $[0, 2]$. The maximum occurs for $\alpha = (\alpha_0 + 1) = 1.3$.

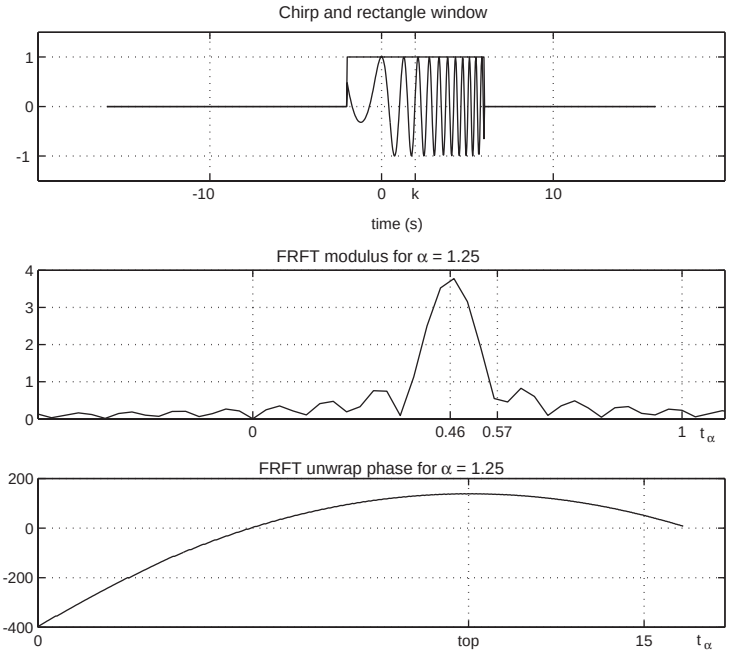

Fig. 3. FRFT of a rectangular windowed linear chirp with parameters: slope $\tan(\alpha_0\pi/2)$ where $\alpha_0 = 0.25$ and offset $\omega_0 = 1$. α ranges $[0, 2]$. The Dirac occurs for $\alpha = (\alpha_0 + 1) = 1.25$.

The first case is a single chirp with noise, used for reference purposes. The second case is composed of two chirps having nonoverlapping time–frequency distributions. In this case the filtering is efficient as it gives the same MSE as in the first case. This confirms that it is possible to separate non overlapping signals

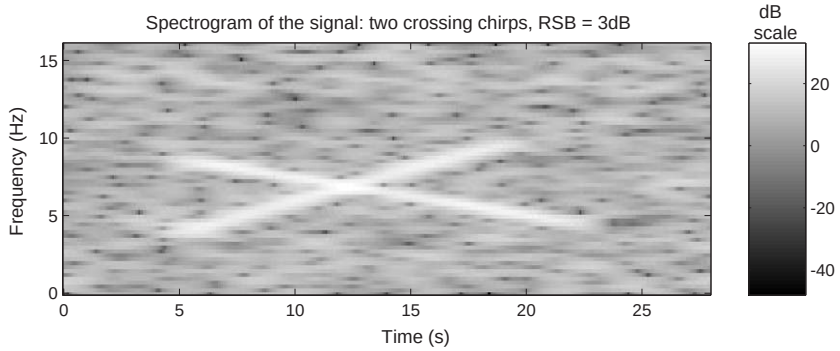

Fig. 4. Spectrogram of the simulation signal.

Table 1
Normalized mean square errors for different signal to noise ratios and different chirp filtering

	Normalized mean square errors		
SNR in dB	One chirp (denoising)	Two disjoints chirps (extraction+ denoising)	Two crossing chirps (separation+ denoising)
$+\infty$	0.0013	0.0013	0.0370
10	0.0173	0.0173	0.0393
3	0.0254	0.0254	0.0515
0	0.0361	0.0361	0.0672
-3	0.0579	0.0579	0.0989
-6	0.1020	0.1020	0.1631
-10	0.2374	0.2374	0.3593

Single chirp filtering (denoising); extraction of one chirp out of two nonoverlapping chirps in the time–frequency plane; separation of one of two crossing chirps in the time–frequency plane.

in the time–frequency plane,for the MSE is only deteriored by the addition of noise.

In the last case, chirps have crossing time–frequency distribution so that separation cannot be performed by the chosen filtering method. In this case, the filtering method only minimizes the influence of each chirp onto the other one, and the MSE raise is due to a local error where the chirps do overlap. Figs. 4 and 5 present the corresponding simulated example. Two crossing chirps are separated and denoised, by appropriate filtering in fractional Fourier domains. Both chirps have different temporal support and have been windowed at their beginning and extinction by halves of 100-taps Hann windows.

Now, we focus on the case of linear chirp filtering and extraction. Due to the concentration property of the chirp transform, it is possible to separate linear chirps from signal or noise. Modern characterization technics use linear chirp analysis as a tool to emphasize nonlinear properties of a system [8]. The use of the FRFT as post-processing in such analysis presents a particular interest in the sense that it allows to separate and analyse individually and more accurately each component of the system response.

3. Propagation in a one-dimensional discrete medium

3.1. Lattice description

A one-dimensional lattice made up of an infinitely long cylindrical waveguide (afterwards refered as pipe) connected to an array of Helmholtz resonators numbered by n is considered. The resonators are connected to the pipe through a pinpoint connection, the radius of the throat's cross sectional area s_n of the nth resonator being assumed to be small compared to the wave length of the acoustic wave ($\sqrt{s_n}/\lambda \ll 1$). Each connection is located along the axis of the pipe by its coordinate z_n with spacing d_n for two consecutive points as shown in Fig. 6.

3.2. General case

In a section of the pipe between two consecutive connection points, the acoustic wave described by the

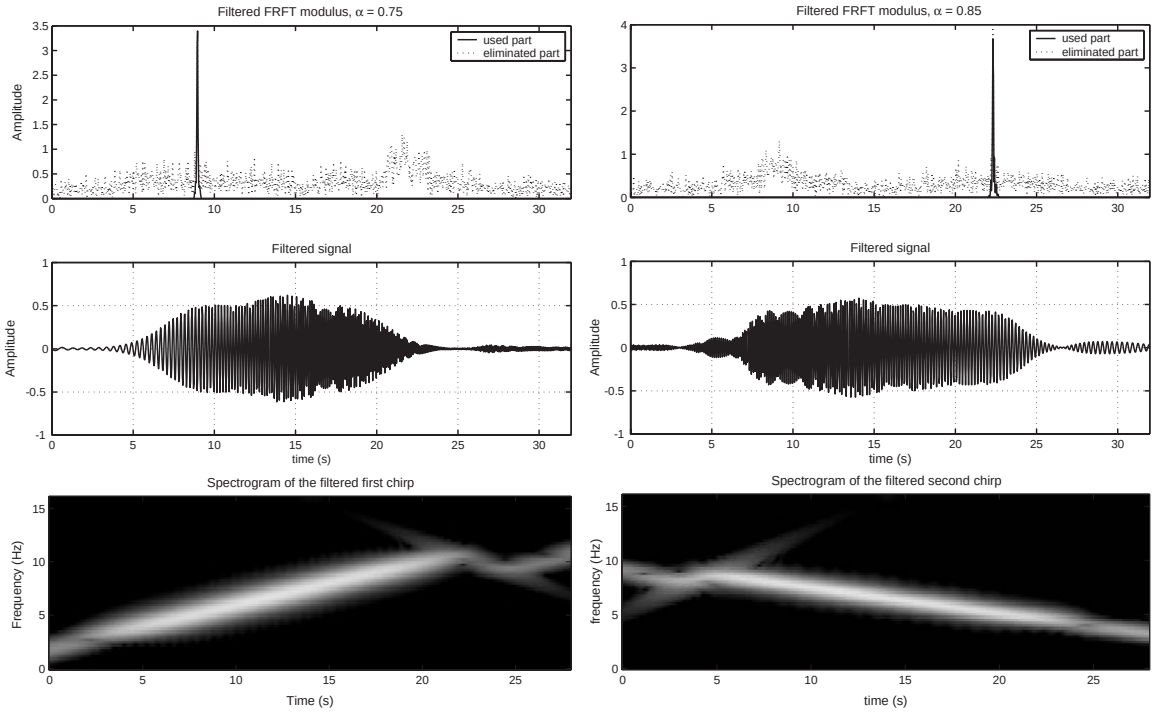

Fig. 5. Chirp extraction and synthesis. Filtering in fractional domains, left column: $\alpha = 0.75$, right column: $\alpha = 0.85$; top) FRFT modulus; middle) time waveforms of the filtered chirp; bottom) spectrograms of the synthesized chirps, same colorscale as in Fig. 4.

pressure $p(z,t)$ and the acoustic velocity $v(z,t)$ is the solution of the wave equation:

$$\frac{\partial^2 p(z,t)}{\partial z^2} - \frac{1}{c^2}\frac{\partial^2 p(z,t)}{\partial t^2} = 0, \tag{18}$$

where c is the sound speed in free space.

At each connection point (Fig. 6), the boundary conditions require the conservation of acoustic flow and continuity of acoustic pressure:

$$v(z,t)|_{z_n^+} - v(z,t)|_{z_n^-} = -\frac{s_n}{S}\, v_t(z_n,t) \quad \text{and}$$

$$p(z,t)|_{z_n^+} = p(z,t)|_{z_n^-}, \tag{19}$$

where $v_t(z_n,t)$ is the acoustic velocity in the throat of the $(n+1)$th resonator. Eqs. (18) and (19) lead to the inhomogeneous wave equation [5]:

$$\frac{\partial^2 p(z,t)}{\partial z^2} - \frac{1}{c^2}\frac{\partial^2 p(z,t)}{\partial t^2} = \sum_n \delta(z - z_n)\,\frac{-\rho s_n}{S}\,\frac{\partial v_t(z,t)}{\partial t}, \tag{20}$$

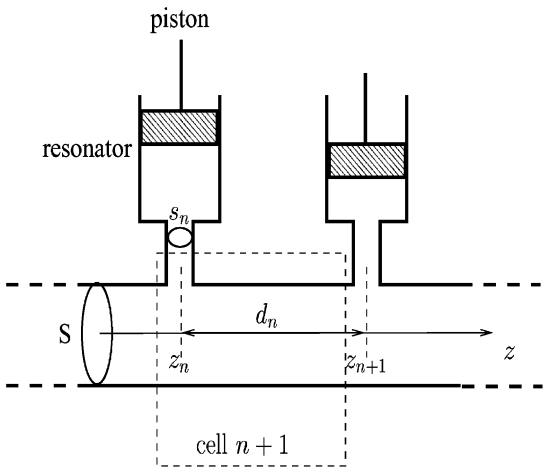

Fig. 6. Experimental set up.

where ρ is the air density. The right hand side term acts as an array of secondary point-sources (scatterers) which work when they are illuminated by the wave travelling in the pipe.

3.3. Propagation in a linear medium

3.3.1. Propagation equation

For a monochromatic acoustic wave with a frequency below the cut-off frequency of the waveguide, the acoustic pressure and velocity along the waveguide are $p(z,t)=p(z)e^{j\omega t}$ and $v(z,t)=v(z)e^{j\omega t}$, where $\omega=kc$ is the angular frequency. In this case Eq. (20) becomes

$$\frac{d^2p(z)}{dz^2}+k^2p(z)=\sum_n \delta(z-z_n)\sigma_n p(z), \tag{21}$$

where $\sigma_n=-j\omega\rho s_n/(SZ_n)$. In this relation Z_n is the impedance of the nth resonator connected at point $z=z_n$ seen from the guide and σ_n is the jump of the pressure derivative $\partial p/\partial z|_{z=z_n}$.

In the linear medium case, the solution of Eq. (21) is seeked by the transfer matrix method [4,5,9]. In the $n+1$th cell ($z_n \leqslant z < z_{n+1}$) the pressure and the velocity are respectively denoted by p_n and v_n and the solution $p_n(z)$ is given as a linear combination of waves travelling in opposite direction:

$$p_n(z)=A_n e^{jk(z-z_n)}+B_n e^{-jk(z-z_n)}, \tag{22}$$

A_n and B_n being, respectively, the amplitudes of the forward and backward waves.

The propagation through one cell is described by

$$V_{n+1}=\mathscr{T}_{n+1}V_n \quad \text{where } V_n=\begin{pmatrix}A_n\\B_n\end{pmatrix}$$

which links the vector pair $(A_n\ B_n)^t$ and $(A_{n+1}\ B_{n+1})^t$. The matrix $\mathscr{T}_{n+1}$ has the following form [5]:

$$\mathscr{T}_n=\begin{pmatrix}\left(1+\dfrac{\sigma_n}{2jk}\right)e^{jkd_n} & \dfrac{\sigma_n}{2jk}e^{-jkd_n}\\ -\dfrac{\sigma_n}{2jk}e^{jkd_n} & \left(1-\dfrac{\sigma_n}{2jk}\right)e^{-jkd_n}\end{pmatrix}. \tag{24}$$

The propagation through the lattice from z_n to z_{n+m} is then described by the relation

$$V_{n+m}=\prod_{i=1}^{m}\mathscr{T}_{n+i}V_n. \tag{25}$$

V_n may be interpreted as the vector of the initial conditions (or boundary conditions) and V_{n+m} is the vector of the wave amplitudes m cells further along.

3.3.2. Periodic lattice

For a periodic lattice, the transfer matrix $\mathscr{T}_n=\mathscr{T}$ and the derivative jump $\sigma_n=\sigma$ are the same ones for each cell. The infinite medium problem is analogous to the Krönig–Penney model well known in solid state physics to investigate the motion of electrons in a periodic potential [4]. So the propagation in the lattice can be seen in terms of plane waves subject to multiple reflections at each derivation, resulting in standing waves. It is also possible to describe the propagation in terms of a collective excitation that propagates in the periodic lattice without scattering but with a modified dispersion relation. The result is that spatial periodicity gives rise to dispersion even in the model of plane waves. In this special case the lattice works as a filter with allowed and forbidden frequency bands.

In the periodic lattice, the dispersion relation takes the form

$$\cos(qd)=\cos(kd)+\frac{\sigma}{2k}\sin(kd), \tag{26}$$

q being the Bloch wave number [2]. This derived dispersion relation exhibits the peculiar characteristic of filters marked by forbidden frequencies or gaps or stopbands and allowed frequencies or passbands in the frequency domain which results from the resonances and the periodic arrangements of the medium. Waves that obey the relation $|\cos(qd)|\leqslant 1$ are within a passband and travel freely in the duct and waves such that $|\cos(qd)|>1$ are in a forbidden band and are quickly damped spatially. They become evanescent so that they cannot propagate.

3.4. Propagation in a ordered lattice with discrete nonlinearities

For high sound level ($\simeq$ 120 dB), the relation between the acoustic pressure and the velocity in the neck of the Helmholtz resonators is no longer linear. A simple model of nonlinear Helmholtz resonator can be developed by using a Taylor's development of the restoring force due to the change of pressure in the resonator cavity.

The air enclosed in the resonator acts as a spring for the lumped mass of air moving within the neck. A general description of the nonlinear behavior of the Helmholtz resonator may be derived by taking into account the quadratic term in the restoring force of the spring. The relative change of the pressure p_n in the

cavity of the nth resonator due to a small displacement x_n of the air in the neck induces a restoring force F_n that has the following form [3]:

$$F_n = p_n s_n = -\frac{\rho c^2 s_n^2}{V_0}\,[x_n - \alpha_n x_n^2 + \mathrm{o}(x_n^3)]. \tag{27}$$

where γ is the specific heat ratio. In this equation $\alpha_n = (\gamma+1)s_n/(2V_0)$ and c is the sound velocity given by $c=\sqrt{\gamma p_0/\rho}$. For a monochromatic wave with a pulsation ω the nonlinear relation between the acoustic pressure p_n and the velocity v_n just outside the opening of the nth resonator is $p_n = Z_n^{\mathrm{NL}} v_n$ where Z^{NL} is the "nonlinear impedance" which takes the form

$$Z_n^{\mathrm{NL}} = Z_n^{\mathrm{L}} + \alpha_n \rho l'_{\mathrm{c}} \frac{\omega_0^2}{\omega^2}\frac{p_n}{Z_n^{\mathrm{L}}} + \mathrm{o}\left(\left(\frac{p_n}{Z_n^{\mathrm{L}}}\right)^2\right), \tag{28}$$

with Z_n^{L} the linear impedance of the nth resonator ($Z_n^{\mathrm{L}} = \mathrm{j}\omega\rho l'_{\mathrm{c}}(1-(\omega_0^2/\omega^2))$) and $\omega_0^2 = s_n c^2/(V_0 l'_{\mathrm{c}})$ the resonance frequency of the Helmholtz resonator and l'_{c} the effective neck length. So, the nonlinear effects lead merely to a additive correction to the linear impedance of the Helmholtz resonator which is non-vanishing only around the Helmholtz resonance ω_0.

So, the propagation of waves in an ordered lattice with discrete nonlinearities is described by Eq. (20) where $v_t(z,t)$ is not a linear function of $p(z,t)$. Nevertheless we assume that the propagation (between two resonators) remains linear. So the pressure in the main pipe is calculated in the same way as for a linear medium but now nonlinear operators describe the scattering of waves at each connection point of the lattice.

4. Experimental results

4.1. Description of the experimental set-up

Fig. 6 shows the experimental setup. It consists of a 8 m length cylindrical pipe having a 5 cm inner diameter and a 0.5 cm thick wall connecting with an array of 60 Helmholtz resonators as side branches. The distance between two consecutive resonators is $d_n = 0.1$ m. The upstream section links this system to a loudspeaker designed for high acoustic power level and used to generate linear frequency modulated waves (chirps) or wavepackets (approximate δ-function). The duration of the chirp is 0.5 s and the frequency range is included in $[100; 600]$ Hz. The wavepackets duration is 0.01 s and its frequency range extends from 0 to 2500 Hz. At the end of the downstream section, an approximately anechoic termination made of plastic foam suppresses reflected waves. Lastly, two microphones m_1 and m_2 (B& K 4136 with Nexus 2690 amplifier) measure the pressure in up and downstream sections. These microphones produce 0.2% of distortion at 150 dB which ensures that the nonlinear effects are generated by the propagation in the lattice (and not by the microphones themself). The data acquisition is carried out by means of a 16 bits AD-converted with a sampling frequency of 10 kHz and an anti-aliasing filter (8th order Chebyschev filter) with a bandwidth of 4 kHz.

All the resonators are identical and are $L = 16.5$ cm long cylindrical cavities with a diameter of 4 cm. Their volumes may be independently tuned by moving pistons. Their neck is a 2 cm length tube having a diameter of 1 cm. The Helmholtz resonance frequency corresponding to the whole volume ($V_0 = 2.1\times10^{-4}$ m^3) is 300 Hz. All the pipes used are stiff enough for their structural modes to be outside the frequency range of interest.

4.2. Results

The Pseudo Wigner–Ville distribution (PWVD) images associated with the propagation of an acoustic pulse in the linear ordered lattice are presented in Fig. 7. Fig. 7a is the PWVD of the signal picked-up in the upstream section of the apparatus by microphone m_1 corresponding to the incident impulse beginning at 0.4 s and three narrow bands reflected signal. Fig. 7b shows the PWVD of the transmitted (output) signal given by microphone m_2. For the case where all the resonators are identical (the resonance frequency is 300 Hz) the waves belonging to the allowed bands are shown at the time 0.49 s (corresponding to the propagation of waves through the lattice) and two kinds of gaps are observed in the PWVD of the transmitted signal (Fig. 7b): the gaps due to the resonators included in [300 : 450] Hz (Helmholtz resonance) and [1100 : 1200] Hz and the gap due to the period of the lattice at 1700 Hz. The waves with frequencies close to the gaps arrive at longer and longer delays. So their group velocity goes to zero as the frequency gets closer to

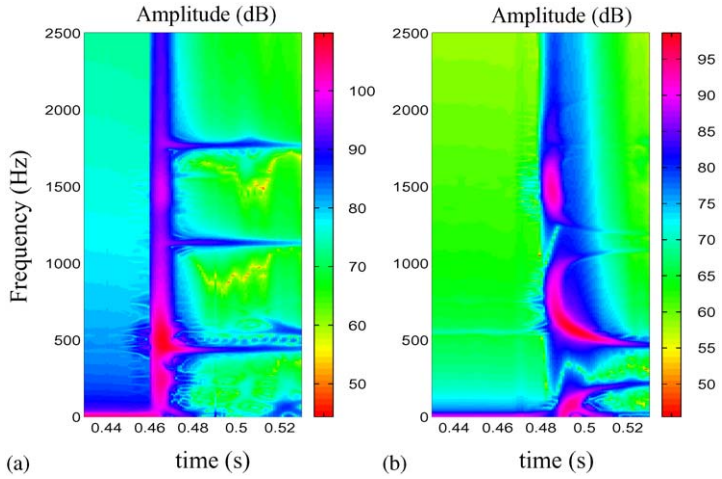

Fig. 7. (a) Wigner–Ville transform of a pulse signal upstream of the lattice. (b) Wigner–Ville transform of a pulse signal downstream of the lattice.

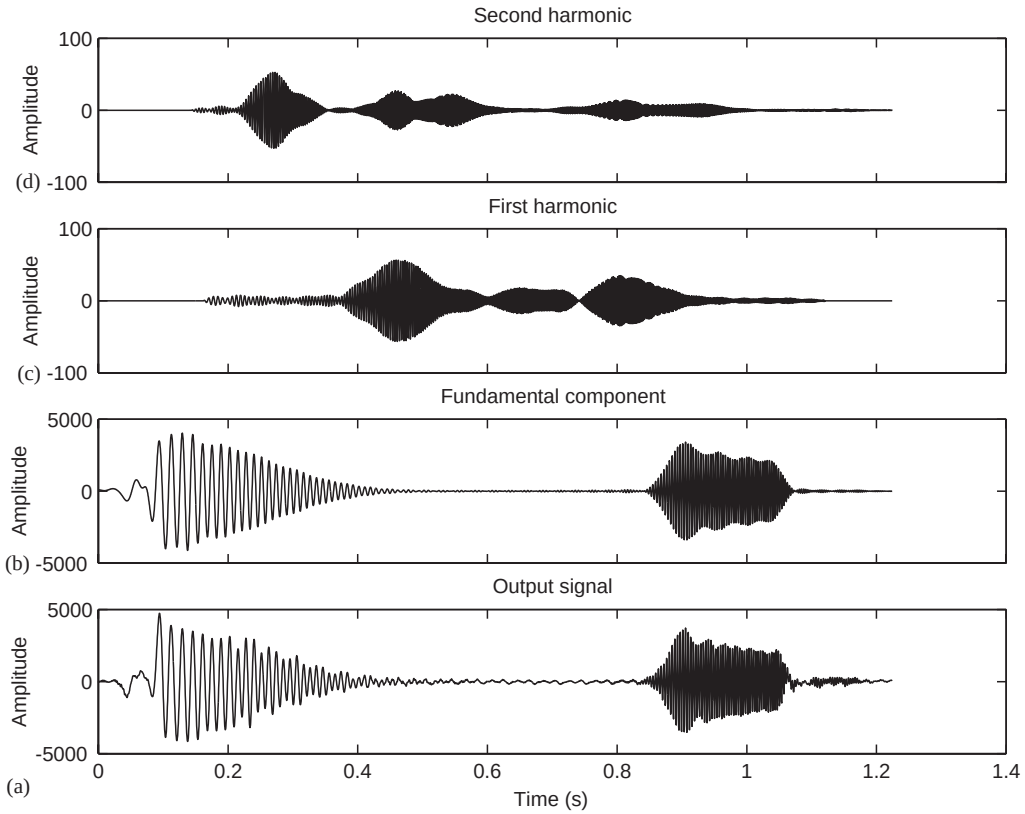

Fig. 8. Time waveforms of (a) transmitted signal downstream of the lattice, (b) fundamental component filtered in domain $\alpha = -0.91$, (c) first harmonic filtered in domain $\alpha = -0.82$, (d) second harmonic filtered in domain $\alpha = -0.74$.

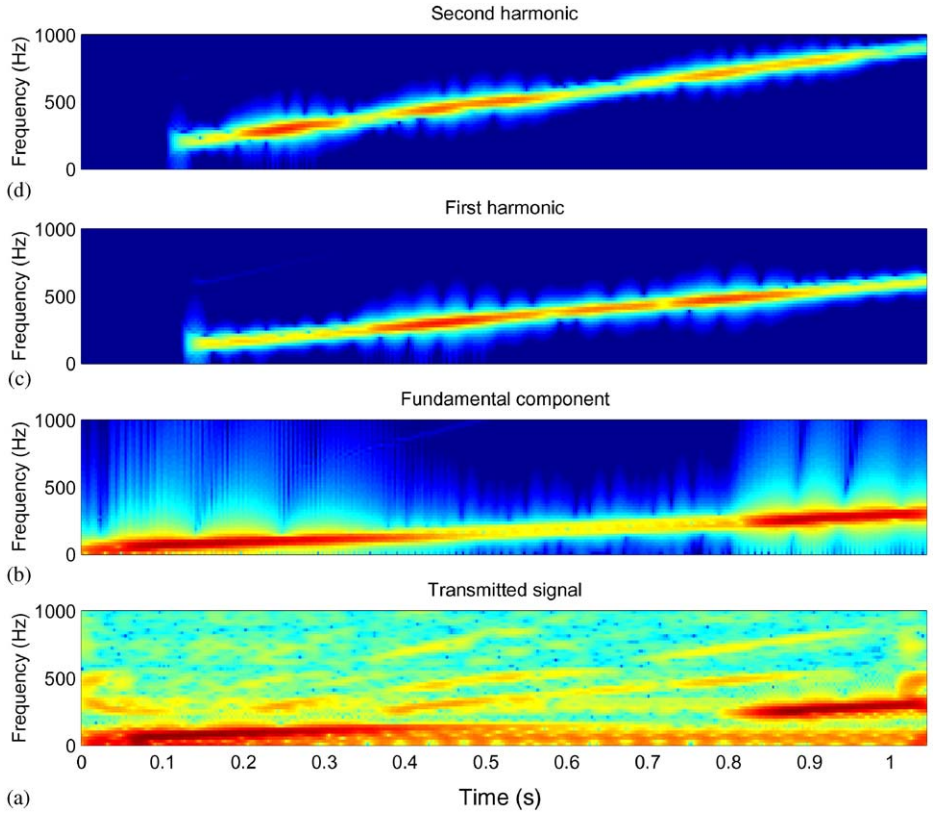

Fig. 9. Spectrograms of (a) transmitted signal downstream of the lattice, (b) fundamental component filtered in domain $\alpha = -0.91$, (c) first harmonic filtered in domain $\alpha = -0.82$, (d) second harmonic filtered in domain $\alpha = -0.74$.

the cutoff frequencies of each gap. This is indicated on the PWVD plot by long tails on each side of the gaps. From the point coordinates of PWVD of the output signal, it is possible to estimate the group velocity as a frequency dependant function which caracterizes the dispersion of the medium.

For high levels of the source, the lattice has a nonlinear response. Since the restoring force of the cavity is no longer a linear function of acoustical pressure, higher harmonics are generated by the interactions of the acoustic wave with the resonators. However, in most cases, the amplitude of the input signal being not large enough, the level of nonlinear effects is quite weak.

Since the mechanisms responsible for the nonlinear effects are various, the several components of such a signal are not equally involved in the generation of harmonics. So, to investigate how the energy is transferred from one monochromatic component to its harmonics, we analyse the behaviour of a linear FM signal in the lattice. The response of the lattice to such a signal is a multicomponent signal made up of chirps each of them corresponding to one harmonic. Their amplitudes are time dependent and display which parts of the signal are involved in the nonlinear process and their relative weights.

For the nonlinear case, the input signal is a linear FM signal with a frequency range (from 100 to 600 Hz) including the first stopband of the lattice ([300 : 450]). The spectrogram of the transmitted signal (Fig. 9a) shows the presence of higher harmonics for the frequencies of the input signal belonging to the forbidden band (the slope of the input chirp is multiplied by 2 and by 3). The chirp extraction method is used to separate the different components of the signal and the results are presented in Figs. 8 and 9.

The fundamental component is found by filtering in the fractional domain defined by $\alpha = -0.91$, the first and second harmonics are obtained respectively with $\alpha = -0.82$ and -0.74.

The temporal signals (Fig. 8) of each component of the transmitted signal show that the contribution of the higher harmonics is small in face of the amplitude of the input signal but becomes quite large in face of the amplitude of fundamental component in a forbidden band. This separation points out the various nonlinear processes existing in a bandgap. For frequencies belonging to the beginning of the stopband (from 0.2 to 0.4 s) only the second harmonic is excited. On the contrary, at the end of the stopband (from 0.6 to 0.85 s) only the first harmonic is important in the propagation of the wave (the fundamental component vanishes). The higher harmonics are equally excited for the duration ranging between 0.4 and 0.6 s. All these differences show the complexity of the physical phenomena which occur.

The spectrograms of each component of the transmitted signal (Fig. 9) show the frequency localization of the transmitted signal energy. The study of these plots shows the first approximation of the nonlinear response of a Helmholtz resonator used in the analytical model. Around the resonance frequency (from 0.4 to 0.6 s) the amplitude of the first harmonic is larger than the amplitude of others harmonics. The model could be improved by including higher order terms. Nevertheless only the second harmonic emerges from the response of lattice for frequencies ranging between 200 Hz and 300 Hz.

5. Conclusion

We have shown that the fractional Fourier transform is well adapted to the analysis of the linear chirp signal. It is found that the transform of such a signal is similar to the transform of a sine for the classical Fourier transform. Simulations have shown that it is possible to extract linear chirps out of multicomponent and noisy signal.

In the considered application, this method is very efficient to display the high intensity sound waves but also to study separately each higher harmonic. The chirp extraction method allows to improve the underlying model. The reconstruction of each harmonic in the time domain is a major tool to the study of energy transfers between the input signal and the harmonics, providing a better understanding of the nonlinear effects on the propagation in dispersive media.

References

[1] L. Almeida, The fractional Fourier transform and time–frequency representations, IEEE Trans. Signal Process. 42 (11) (1994) 3084–3091.
[2] F. Bloch, Der quantenmechanik electronishen, Z. Physik 55 (1928) 555.
[3] R.R. Boullosa, F.O. Bustamante, The reaction force on a Helmholtz resonator driven at high sound pressure amplitudes, Amer. J. Phys. 60 (8) (1992) 722–726.
[4] F.J. Dyson, The dynamics of a disordered linear chain, Phys. Rev. 92 (6) (1953) 1331–1338.
[5] H. Levine, Unidirectional Wave Motion, North-Holland, New York, 1978.
[6] V. Namias, The fractional order Fourier transform and its application to quantum mechanics, J. Inst. Math. Appl. (25) (1980) 241–265.
[7] H. Ozaktas, O. Arikan, A. Kutay, G. Bozdağı, Digital computation of the fractional Fourier transform, IEEE Trans. Signal Process. 44 (9) (1994) 2141–2150.
[8] O. Richoux, C. Depollier, J. Hardy, Characterization by a time–frequency method of classical waves propagation in one-dimensional lattice: effects of the dispersion and localized nonlinearities, Acta Acustica united with Acustica 88 (2002) 934–941.
[9] N. Sugimoto, Dispersion characteristics of sound waves in a tunnel with an array of Helmholtz resonators, J. Acoust. Soc. Amer. 97 (3) (1994) 1446–1459.